Hindawi
Advances in Condensed Matter Physics
Volume 2021, Article ID 3914210, 16 pages
https://doi.org/10.1155/2021/3914210

Research Article

A Novel Elastic Metamaterial with Multiple Resonators for Vibration Suppression

Saman Ahmadi Nooraldinvand,[1] Hamid M. Sedighi ,[1,2] and Amin Yaghootian[1]

[1]*Mechanical Engineering Department, Faculty of Engineering, Shahid Chamran University of Ahvaz, Ahvaz, Iran*
[2]*Drilling Center of Excellence and Research Center, Shahid Chamran University of Ahvaz, Ahvaz, Iran*

Correspondence should be addressed to Hamid M. Sedighi; h.msedighi@scu.ac.ir

Received 6 April 2021; Accepted 19 May 2021; Published 2 June 2021

Academic Editor: Shengxuan Xia

In this paper, two models of elastic metamaterial containing one and two resonators are proposed to obtain the bandgaps with the aim of providing broadband vibration suppression. The model with one DOF is built by assembling several unite cells in which each unite cell consists of a rectangular frame as the base structure and a rack-and-pinion mechanism that is joined to the frame with a linear spring on both sides. In the second model with two DOF, a small mass is added while its center is attached to the center of the pinion on one side and the other side is connected to the rectangular frame via a linear spring. In the first mechanism, the pinion is considered as the single resonator, and in the 2DOF model, on the other hand, the pinion and small mass acted as multiple resonators. By obtaining the governing equations of motion for a single cell in each model, the dynamic behavior of two metastructures is thoroughly investigated. Therefore, the equations of motion for the two models are written in matrix form, and then, the dispersion relations are presented to analyze the influences of system parameters on the bandgaps' starting/ending frequencies. Finally, two models are successfully compared and then numerically simulated via MATLAB-SIMULINK and MSC-ADAMS software. With the aid of closed-form expressions for starting/ending frequencies, the correlation between the system parameters and bandgap intervals can be readily recognized.

1. Introduction

Metamaterials are referred to the types of advanced materials that are synthetically made including small substructures which generally behave like a continuous material. The frequency bands at which acoustic and elastic waves cannot propagate are called bandgap, which is the most prominent feature of metamaterials. The propagation of waves of different wavelengths is controlled by the low/high-frequency bandgaps generated by the metamaterials. Given this unique property, metamaterials can be used in the field of acoustic insulation, filtration of waves, oscillations reduction, and sonic transmission [1–3]. The cell body of an acoustic metamaterial consists of a basic structure in which one or more locally vibrating components are located. Interactions between the base environment and local vibrators enable interesting physical phenomena such as bandwidth, negative effective density, negative modulus of elasticity, directional filtering and wave conduction, increased dissipation, and vibroacoustic attenuation [4, 5]. Basically, two types of local resonators are used: (1) translational resonator and (2) rotary resonator, which cause negative effective density and negative effective elastic modulus, respectively [6]. Huang et al. [7] demonstrated the consequence of using different equivalent models to represent a lattice system consisting of mass-in-mass units. Then they studied the dispersive wave propagation and compared to various equivalent models. They found that, if the classical elastic continuum is utilized to represent the original mass-in-mass structure, the effective mass density will be frequency dependent and may become negative for frequencies near the resonance frequency of the internal mass. In the meantime, if a multi-

displacement microstructure continuum model is utilized, the dispersive behavior of wave propagation and the band gap structure can be adequately described.

Active and passive periodic structures are made up of similar substructures or unit cells that are joined to each other in a similar way. The periodicity of these structures exhibits unique dynamic properties because they can prevent wave propagation and act as a mechanical filter [8]. Wave propagation is not possible in infinite periodic structures at particular frequency intervals. Photonic bandgaps are frequency bands in which acoustic/elastic waves cannot be transmitted. Unlike infinite periodic structures, wave transmission or vibration occurs sparingly if finite periodic structures are excited within the band gaps, which can be examined for frequency response function diagrams to obtain this wave or vibration transmission [9]. Propagation or passbands allow waves along these structures which propagate in certain frequency ranges without attenuation; and stopbands, attenuation bands, or bandgaps are the frequency bands in which waves can be attenuated [10]. In periodic structures, two common methods for generating phononic bandgaps are Bragg scattering and local resonances [9]. The band structure and wave reduction mentioned above are due to these two types of mechanisms that are clearly different from each other [11]. In the high-frequency mode, Bragg bandgaps can be used to filter the waves, but in the low-frequency mode, this is not possible [12]. On the other hand, at much lower frequencies than Bragg scattering, bandgaps can be created by local resonance [9]. Control of resonant-type bandgaps due to local resonance (LR) mechanism is easily possible, unlike Bragg-type bandgaps. In order to adjust the bandgap properties, the properties of the locally resonant structure can be changed. Chen and Chien [12] proposed a mass grid system, and before this new idea was applied to the field of elastic, it was presented in the field of acoustic.

Lazarov and Jensen [10] conducted their study in both linear and nonlinear modes to propagate the wave in one-dimensional chains in which nonlinear oscillators are joined. They found that in the nonlinear state, the bandgap could shift depending on the amplitude and degree of local nonlinearities. Also, the results of their research showed that in the linear mode, the location of the gap is around the resonant frequency which allows the gap to be generated at a lower frequency domain. Casalotti et al. [13] examined an Euler-Bernoulli beam with an arrangement of nonlinear mass-spring substructures attached to investigate the ability of the nonlinear metamaterial beam to absorb multistate vibrations. Beam-connected substructures that act as local resonators or vibration absorbers created bandgaps. At first, they identified the frequency stop bands of the unite cell, and then in order to investigate the multifrequency stopband, the frequency response for the nonlinear metamaterial beam was extracted. They indicated that, for the metamaterial beam, the oscillations related to the lowest three vibration modes were significantly reduced by properly adjusting the constituent parameters of local absorbers. Zhou et al. [14] presented two models of an acoustic metamaterial beam in which local resonators were attached owning to both flexible bandgaps and high static stiffness. Initially, an equivalent model by mass-spring-beam of acoustic metamaterial beam with variable cross section was considered and analyzed analytically. The dispersion relationship of acoustic metamaterial beam was extracted, and the effect of different control parameters on bandgaps was investigated. Then, they simulated and examined a two-dimensional finite element model of acoustic metamaterial beam for the sake of validation in COMSOL Multiphysics. Their results showed that there is good compatibility between the analytical model and the two-dimensional model. Finally, a three-dimensional model of acoustic metamaterial beam was presented and discussed in two forms of equal and unequal thickness to measure the wave attenuation. Huang and Sun [15] studied a multiresonator mass-in-mass grid system and obtained its dispersion curves and bandgap. It was shown that bandgap can be displaced by changing the magnitude of the internal masses and the spring constant. They proposed a monoatomic model equivalent to the original system and found that the effective mass at bandgaps frequencies is negative. Finally, they introduced a microstructure continuous model that can obtain the dispersive behavior and bandgap structure of the original system. According to the study conducted by Sun et al. [16], it was shown that an acoustic absorber based on metamaterial can be thought of as a uniform isotropic beam with a number of very small mass-spring subsystems at different points. They also discussed how to create bandgap by subsystems, the negative effective mass, and stiffness. Their results showed that common mechanical vibration absorbers are the basis of the actual working mechanism of metamaterial beam. Shear forces and bending moments were then created to hold the beam straight and prevent wave propagation. An important and in-depth topical review in the field of active metamaterials and metadevices was performed by Xiao et al. [17]. They reported the advancement of active metadevices and metamaterials ranging from microwave to visible wavelengths, including milestones as well as the state of the art, and finally presented the future prospects together with several emerging tuning strategies and materials.

Most studies of metamaterial models are based on a damper-spring-damper combination. However, this paper uses a new combination of rack-and-pinion mechanism and mass to achieve wider bandgaps and investigate the dynamic behavior of the new combination. In the current research, two models of elastic metamaterials are proposed to obtain broadband bandgaps for vibration suppression. The models are made from a combination of a rack-and-pinion mechanism connected to a concentrated mass. The governing equations of both models with one and two degrees of freedom are solved by MATLAB-SIMULINK and dispersion curves and frequency response diagrams are also drawn. Then, the effect of control parameters on the starting and ending frequencies of the bandgaps is mathematically investigated. Finally, both models are modeled and simulated in MSC-ADAMS software, and the

desired graphs are numerically extracted. There is a satisfactory agreement between the simulated results and those obtained by numerical algorithms.

2. Models: 1DOF and 2DOF

In this section, two models consisting of one- and two-degree-of-freedom elastic metamaterials (EMM) are introduced and discussed. The models include rectangular cells containing a rack-and-pinion mechanism and a concentrated mass. The presence of a rack prevents slipping between the pinion and the cell which converts the transfer motion to a pure rolling motion. The aim of this study is to analytically obtain the bandgaps of the proposed models in order to reduce or eliminate the mechanical vibrations. For both one- and two-degree-of-freedom models, the mathematical models are presented and the staring/ending frequencies of bandgaps are mathematically extracted with close-form expressions.

2.1. One DOF Model of EMM

2.1.1. One DOF Model: Mathematical Formulation. The proposed one-degree-of-freedom model of elastic metamaterials is shown in Figure 1. As shown, the main body of this model consists of rectangular frames with a rack-and-pinion inside. Rectangular frames are then connected by linear springs. On the other hand, the pinion is connected to the walls of the rectangular frame by two linear springs.

The parameters defined for the problem are shown in Figure 2, which represents the unit cell of the one-degree-of-freedom model. Therefore, using Newton's second law, the governing equations of a unit cell are derived as follows:

$$\sum F_x = m_1\ddot{x}_n \Rightarrow -k_1\left(x_n - x_{n-1}\right) - k_1\left(x_n - x_{n+1}\right) - m_2\left(\ddot{x}_n + r\ddot{\theta}\right) = m_1\ddot{x}_n, \tag{1}$$

$$\sum M_O = I_O\ddot{\theta} \Rightarrow -2k_2\left(r\theta\right)r - m_2\left(\ddot{x}_n\right)r = I_O\ddot{\theta}, \tag{2}$$

where m_1 and m_2 are frame and pinion masses, respectively, $r$andθ are the radius and the rotational displacement of pinion, respectively, x_n represents the translational displacement of the nth cell, and I_O denotes the mass moment of inertia of the pinion with respect to the point o.

Now, Equations (1) and (2) are written in a matrix form as follows:

$$\begin{bmatrix} m_1 + m_2 & m_2 r \\ m_2 r & I_O \end{bmatrix}\begin{bmatrix} \ddot{x}_n & \ddot{\theta} \end{bmatrix} + \begin{bmatrix} 2k_1 & 0 \\ 0 & 2k_2 r^2 \end{bmatrix}\begin{bmatrix} x_n \\ \theta \end{bmatrix} + \begin{bmatrix} -k_1\left(x_{n-1} + x_{n+1}\right) \\ 0 \end{bmatrix} = \begin{bmatrix} 0 \\ 0 \end{bmatrix}, \tag{3}$$

and the dimensionless parameters used in this model are defined by

$$\begin{aligned} M &= \frac{m_1}{m_2}, \\ \widehat{I} &= \frac{I_O}{m_2 r^2}, \\ \widehat{K} &= \frac{k_1}{k_2}, \\ \widehat{\omega}_n &= \sqrt{\frac{k_2}{m_2}}, \\ r\overline{x}_n &= x_n, \\ \tau &= \omega t, \\ \widetilde{\omega} &= \frac{\omega}{\widehat{\omega}_n}, \end{aligned} \tag{4}$$

where $\widehat{\omega}_n$ is the local natural frequency, $M, \widehat{I}, \widehat{K}, \overline{x}_n, \tau$, and $\widetilde{\omega}$ are the dimensionless mass, moment of inertia, stiffness, displacement, time, and frequency, respectively. By replacing these dimensionless parameters in Equation (3), the new form of governing equations can be written as follows:

$$\begin{bmatrix} (M+1)\widetilde{\omega}^2 & \widetilde{\omega}^2 \\ \widetilde{\omega}^2 & \widehat{I}\widetilde{\omega}^2 \end{bmatrix}\begin{bmatrix} \dfrac{d^2\overline{x}_n}{d\tau^2} \\ \dfrac{d^2\theta}{d\tau^2} \end{bmatrix} + \begin{bmatrix} 2\widehat{K} & 0 \\ 0 & 2 \end{bmatrix}\begin{bmatrix} \overline{x}_n \\ \theta \end{bmatrix} + \begin{bmatrix} -\widehat{K}\left(\overline{x}_{n-1} + \overline{x}_{n+1}\right) \\ 0 \end{bmatrix} = \begin{bmatrix} 0 \\ 0 \end{bmatrix}. \tag{5}$$

2.1.2. One DOF Model: Dispersion Properties. In this section, the solution corresponding to the harmonic wave for the

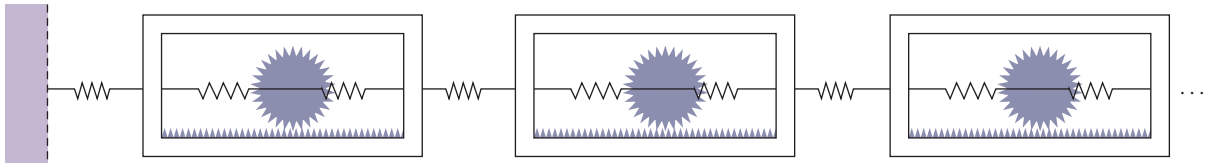

Figure 1: A schematic of the metamaterial arrangement of the 1DOF model.

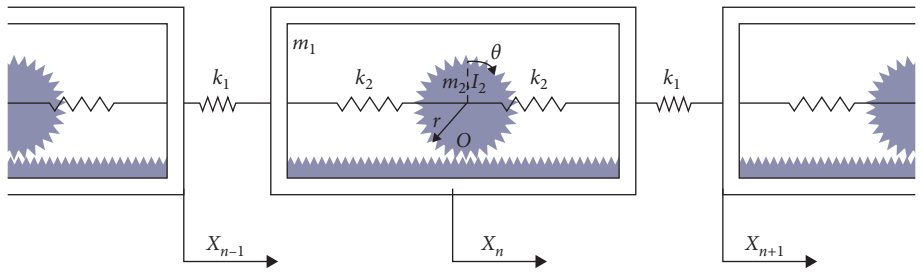

Figure 2: A schematic of a unite cell of the 1DOF model.

1DOF model is defined for extracting the dispersion relations and the bandgap frequencies:

$$\begin{bmatrix} \overline{x}_n \\ \theta \end{bmatrix} = \begin{bmatrix} \overline{x}_n^{\circ} \\ \theta^{\circ} \end{bmatrix} e^{i(\mathrm{qa}.n+\tau)} + c.c, \qquad [\overline{x}_{n\pm1}] = [\overline{x}_{n\pm1}^{\circ}] e^{i(\mathrm{qa}.n+\tau)} + c.c, \tag{6}$$

where $\overline{x}_n^{\circ}$ and θ° are the steady-state amplitude of the solution, qa is the phase factor, and $n$represents the periodic number. Moreover, $a.n$ indicates the distance between $n$thcell from the origin (support) [18–22]. Substituting Equations (6) into (5), the new form of the governing equation in its matrix form is as follows:

$$\begin{bmatrix} (M+1)\widetilde{\omega}^2 & \widetilde{\omega}^2 \\ \widetilde{\omega}^2 & \widehat{I}\widetilde{\omega}^2 \end{bmatrix} \begin{bmatrix} \overline{x}_n^{\circ}(-1)e^{i(\mathrm{qa}.n+\tau)} + c.c \\ \theta^{\circ}(-1)e^{i(\mathrm{qa}.n+\tau)} + c.c \end{bmatrix} + \begin{bmatrix} 2\widehat{K} & 0 \\ 0 & 2 \end{bmatrix} \begin{bmatrix} \overline{x}_n^{\circ} e^{i(\mathrm{qa}.n+\tau)} + c.c \\ \theta^{\circ} e^{i(\mathrm{qa}.n+\tau)} + c.c \end{bmatrix} + \begin{bmatrix} -\widehat{K}\left(\overline{x}_n^{\circ} e^{i\mathrm{qa}(n-1)} e^{i\tau} + \overline{x}_n^{\circ} e^{i\mathrm{qa}(n+1)} e^{i\tau} + c.c\right) \\ 0 \end{bmatrix} = \begin{bmatrix} 0 \\ 0 \end{bmatrix}. \tag{7}$$

Now, by factoring and arranging the different expressions in Equation (7), the final form of the equations of motion for the considered system is given by

$$\begin{bmatrix} -(M+1)\widetilde{\omega}^2 + 2\widehat{K} - \widehat{K}(2\cos(\mathrm{qa})) & -\widetilde{\omega}^2 \\ -\widetilde{\omega}^2 & -\widehat{I}\widetilde{\omega}^2 + 2 \end{bmatrix} \begin{bmatrix} \overline{x}_n^{\circ} \\ \theta^{\circ} \end{bmatrix} e^{i(\mathrm{qa}.n+\tau)} + c.c = \begin{bmatrix} 0 \\ 0 \end{bmatrix}. \tag{8}$$

The dispersion relation for the 1DOF model can be obtained from Equation (8). For a nontrivial solution, the determinant of the coefficient matrix must be equal to zero. Therefore, the dispersion relation is extracted as

$$(\widehat{I}(1+M)-1)\widetilde{\omega}^4 + 2(-M-1-\widehat{I}\widehat{K}(1+\cos(\mathrm{qa})))\widetilde{\omega}^2 + 4\widehat{K}(1-\cos(\mathrm{qa})) = 0. \tag{9}$$

By solving Equation (9) for $\widetilde{\omega}$, the relation for the acoustic and optical frequencies of the EMM can be achieved as described in Equations (10) and (11). Then, by employing the obtained closed-form expressions, the dispersion curves for the 1DOF model are shown in Figure 3.

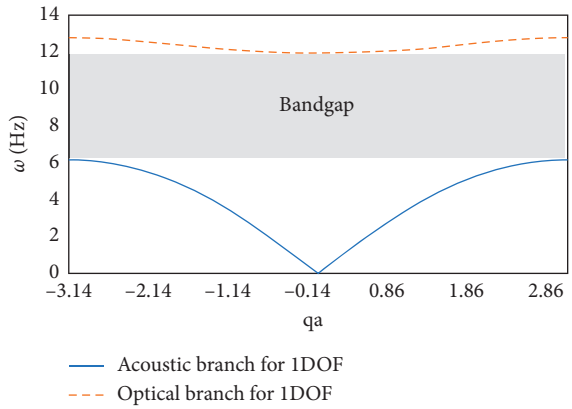

Figure 3: Dispersion curves for the 1DOF model.

where

$$\widetilde{\omega}_{\text{Acoustic}} = \sqrt{\frac{\Delta - \sqrt{\Phi}}{\Psi}}, \tag{10}$$

$$\widetilde{\omega}_{\text{Optical}} = \sqrt{\frac{\Delta + \sqrt{\Phi}}{\Psi}}, \tag{11}$$

$$\begin{aligned}
\Delta &= M + \widehat{I}\widehat{K} - \widehat{I}\widehat{K}\cos(\text{qa}) + 1,\\
\Psi &= \widehat{I} + \widehat{I}M - 1,\\
\Phi &= \widehat{I}^2\widehat{K}^2\cos^2(\text{qa}) + \left(-2\widehat{I}^2\widehat{K}^2 + 4\widehat{I}\widehat{K} - 4\widehat{K}\right)\cos(\text{qa}) + (1 + 4\widehat{K} + 2M - 2\widehat{I}\widehat{K} - \widehat{I}\widehat{K}M).
\end{aligned} \tag{12}$$

Equations (10) and (11) express the acoustic and optical frequency branches, respectively. Low-frequency and high-frequency dispersive curves are then presented by $\widetilde{\omega}_{\text{Acoustic}}$ and $\widetilde{\omega}_{\text{Optical}}$, respectively [1]. In the above equations, at the point of qa = $\pm\pi$, the slope of the dispersion curve, namely, the velocity of the traveling wave, is equal to zero. This means the wave cannot propagate, similar to what happened at the bandgaps. This area is the first Brillouin zone's boundary. Hence, substituting qa = π and qa = 0 into Equations (10) and (11), and then solving these expressions, the starting and ending frequencies of the bandgaps for the 1DOF model are extracted [1, 20].

2.2. Two DOF Model of EMM

2.2.1. Two DOF Model: Mathematical Formulation. In this section, a model of two degrees of freedom of EMM is presented (see Figure 4). This model is an extended model of the first model discussed in the previous section. The unite cell of the model is made of rectangular frames with a rack-and-pinion inside it connected to a concentrated mass. As shown in Figure 5, the pinion and concentrated mass are joined to the rectangular frame by a linear spring with stiffness of k_2. In addition, the rectangular frames are connected to each other by a linear spring with stiffness of k_1 and create an integrated metastructure. Therefore, the governing equations of a unit cell can be described as follows:

$$\sum F_x = m_1\ddot{x}_n \Rightarrow -k_1(x_n - x_{n-1}) - k_1(x_n - x_{n+1}) - m_2\left(\ddot{x}_n + r\ddot{\theta}\right) - m_3(\ddot{x}_n + \ddot{x}) = m_1\ddot{x}_n, \tag{13}$$

$$\sum M_O = I_O\ddot{\theta} \Rightarrow -2k_2(r\theta)r + (k_2x)r - m_2(\ddot{x}_n)r = I_O\ddot{\theta}, \tag{14}$$

$$\sum F_x = m_3\ddot{x} \Rightarrow -m_3\ddot{x}_n - 2k_2x + k_2r\theta = m_3\ddot{x}, \tag{15}$$

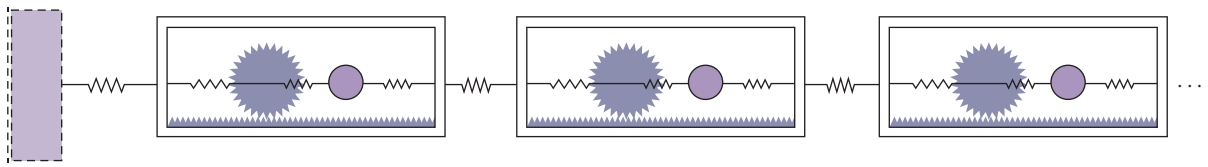

Figure 4: A schematic of the metamaterial arrangement of the 2DOF model.

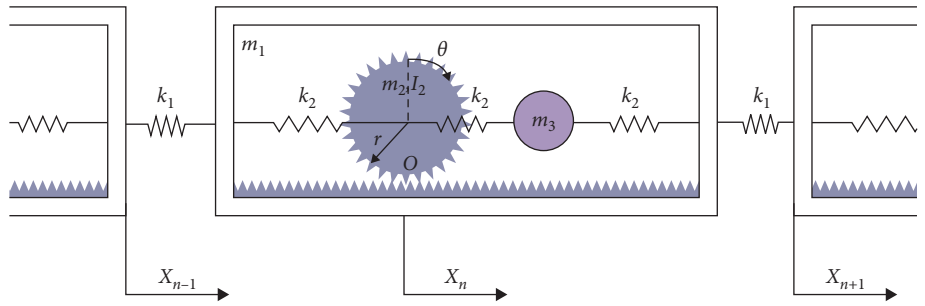

Figure 5: A schematic of a unite cell of 2DOF model.

where $m_3$is the concentrated mass, and x denotes the translational displacement of concentrated mass.

Now, Equations (13) to (15) are written in matrix form as follows:

$$\begin{bmatrix} m_1+m_2+m_3 & m_2 r & m_3 \\ m_2 r & I_O & 0 \\ m_3 & 0 & m_3 \end{bmatrix} \begin{bmatrix} \ddot{x}_n \\ \ddot{\theta} \\ \ddot{x} \end{bmatrix} + \begin{bmatrix} 2k_1 & 0 & 0 \\ 0 & 2k_2 r^2 & -k_2 r \\ 0 & -k_2 r & 2k_2 \end{bmatrix} \begin{bmatrix} x_n \\ \theta \\ x \end{bmatrix} + \begin{bmatrix} -k_1 (x_{n-1} + x_{n+1}) \\ 0 \\ 0 \end{bmatrix} = \begin{bmatrix} 0 \\ 0 \\ 0 \end{bmatrix}. \tag{16}$$

To express the problem in the dimensionless form, the following nondimensional parameters are defined for the 2DOF model:

$$\begin{aligned} \overline{m}_1 &= \frac{m_2 + m_3}{m_1}, \\ \overline{m}_2 &= \frac{m_2}{m_1}, \\ \overline{I} &= \frac{I_O}{m_2 r^2}, \\ \overline{K} &= \frac{k_2}{k_1}, \\ \omega_{n1} &= \sqrt{\frac{k_1}{m_1}} \\ \omega_{n2} &= \sqrt{\frac{2k_2}{m_3}}, \end{aligned}$$

$$\begin{aligned} r\overline{x}_n &= x_n, \\ r\overline{x} &= x, \\ \tau &= \omega t, \\ \overline{\omega}_1 &= \frac{\omega}{\omega_{n1}}, \\ \overline{\omega}_2 &= \frac{\omega}{\omega_{n2}}, \end{aligned} \tag{17}$$

where ω_{n1} and ω_{n2} stand for the natural local frequencies of the first and second modes, respectively, $\overline{m}_1$ and $\overline{m}_2$ are defined as the ratio of the total mass of the pinion and the concentrated mass to the mass of the rectangular frame and pinion-to-frame mass ratio, respectively, $\overline{I}, \overline{K}, \overline{x}_n, \overline{x}$, and τ are the dimensionless moment of inertia, stiffness, displacement for cell, displacement for concentrated mass, and dimensionless time, and $\overline{\omega}_1$ and $\overline{\omega}_2$ denote the first and second dimensionless frequencies, respectively. Using the introduced dimensionless parameters, Equation (16) can be rewritten in a dimensionless form as follows:

$$\begin{bmatrix} (1+\overline{m}_1)\overline{\omega}_1^2 & \overline{m}_2\overline{\omega}_1^2 & (\overline{m}_1-\overline{m}_2)\overline{\omega}_1^2 \\ \overline{\omega}_1^2 & \overline{I}\overline{\omega}_1^2 & 0 \\ \overline{\omega}_2^2 & 0 & \overline{\omega}_2^2 \end{bmatrix} \begin{bmatrix} \dfrac{d^2\overline{x}_n}{d\tau^2} \\ \dfrac{d^2\theta}{d\tau^2} \\ \dfrac{d^2\overline{x}}{d\tau^2} \end{bmatrix} + \begin{bmatrix} 2 & 0 & 0 \\ 0 & \dfrac{2\overline{K}}{\overline{m}_2} & -\dfrac{\overline{K}}{\overline{m}_2} \\ 0 & -\dfrac{1}{2} & 1 \end{bmatrix} \begin{bmatrix} \overline{x}_n \\ \theta \\ \overline{x} \end{bmatrix} + \begin{bmatrix} -(\overline{x}_{n-1}+\overline{x}_{n+1}) \\ 0 \\ 0 \end{bmatrix} = \begin{bmatrix} 0 \\ 0 \\ 0 \end{bmatrix}. \tag{18}$$

2.2.2. Two DOF Model: Dispersion Properties. In this section, the solutions corresponding to the harmonic wave for the 2DOF model are presented as follows for extracting the dispersion relations as well as the bandgap frequencies:

$$\begin{bmatrix} \overline{x}_n \\ \theta \\ \overline{x} \end{bmatrix} = \begin{bmatrix} \overline{x}_n^\circ \\ \theta^\circ \\ \overline{x}^\circ \end{bmatrix} e^{i(\mathrm{qa}.n+\tau)} + c.c, \qquad [\overline{x}_{n\pm1}] = [\overline{x}_{n\pm1}^\circ] e^{i(\mathrm{qa}.n+\tau)} + c.c. \tag{19}$$

Similar to the previous section, $\overline{x}_n^\circ$, θ°, and $\overline{x}^\circ$ represent the steady-state amplitude of the solutions. Substituting Equations (19) into (18), the new forms of the governing equations using matrix notation are given by

By simplifying Equation (1), the final form of the governing equations yields

$$\begin{bmatrix} (1+\overline{m}_1)\overline{\omega}_1^2 & \overline{m}_2\overline{\omega}_1^2 & (\overline{m}_1-\overline{m}_2)\overline{\omega}_1^2 \\ \overline{\omega}_1^2 & \overline{I}\overline{\omega}_1^2 & 0 \\ \overline{\omega}_2^2 & 0 & \overline{\omega}_2^2 \end{bmatrix} \begin{bmatrix} \overline{x}_n^\circ\,(-1)e^{i(\mathrm{qa}.n+\tau)} + c.c \\ \theta^\circ\,(-1)e^{i(\mathrm{qa}.n+\tau)} + c.c \\ \overline{x}^\circ\,(-1)e^{i(\mathrm{qa}.n+\tau)} + c.c \end{bmatrix}$$

$$+ \begin{bmatrix} 2 & 0 & 0 \\ 0 & \dfrac{2\overline{K}}{\overline{m}_2} & -\dfrac{\overline{K}}{\overline{m}_2} \\ 0 & -\dfrac{1}{2} & 1 \end{bmatrix} \begin{bmatrix} \overline{x}_n^\circ e^{i(\mathrm{qa}.n+\tau)} + c.c \\ \theta^\circ e^{i(\mathrm{qa}.n+\tau)} + c.c \\ \overline{x}^\circ e^{i(\mathrm{qa}.n+\tau)} + c.c \end{bmatrix} + \begin{bmatrix} -\left(\overline{x}_n^\circ e^{i\mathrm{qa}(n-1)}e^{i\tau} + \overline{x}_n^\circ e^{i\mathrm{qa}(n+1)}e^{i\tau} + c.c\right) \\ 0 \\ 0 \end{bmatrix} = \begin{bmatrix} 0 \\ 0 \\ 0 \end{bmatrix}. \tag{20}$$

$$\begin{bmatrix} -(1+\overline{m}_1)\overline{\omega}_1^2 + 2 - 2\cos(\mathrm{qa}) & -\overline{m}_2\overline{\omega}_1^2 & -(\overline{m}_1-\overline{m}_2)\overline{\omega}_1^2 \\ -\overline{\omega}_1^2 & -\overline{I}\overline{\omega}_1^2 + \dfrac{2\overline{K}}{\overline{m}_2} & -\dfrac{\overline{K}}{\overline{m}_2} \\ -\overline{\omega}_2^2 & -\dfrac{1}{2} & 1-\overline{\omega}_2^2 \end{bmatrix} \begin{bmatrix} \overline{x}_n^\circ \\ \theta^\circ \\ \overline{x}^\circ \end{bmatrix} e^{i(\mathrm{qa}.n+\tau)} + c.c = \begin{bmatrix} 0 \\ 0 \\ 0 \end{bmatrix}. \tag{21}$$

Dispersion relation for the 2DOF model can be then obtained by manipulating Equation (21). For a nonzero solution, the determinant of the coefficient matrix should be set to zero. Therefore, the dispersion relation is extracted as follows:

$$A\omega^6 + \left(B\omega_{n1}^2 + C\omega_{n2}^2\right)\omega^4 + \left(D\omega_{n1}^2\omega_{n2}^2 + E\omega_{n1}^4\right)\omega^2 + F = 0, \tag{22}$$

where

$$
\begin{aligned}
A &= 2\overline{m}_2\left(\overline{m}_2\overline{I} - 1 - \overline{I}\right),\\
B &= -2\overline{K}\left(2 + \overline{m}_2\right) + 4\overline{m}_2\overline{I}\left(1 - \cos\left(\mathrm{qa}\right)\right),\\
C &= \overline{m}_2\left(\overline{m}_2 + 2\overline{I}\right) + \overline{m}_1\overline{m}_2\left(1 + 2\overline{I}\right),\\
D &= 3\overline{K}\left(1 + \overline{m}_1\right) - 4\overline{m}_2\overline{I}\left(1 - \cos\left(\mathrm{qa}\right)\right),\\
E &= 8\overline{K}\left(1 - \cos\left(\mathrm{qa}\right)\right),\\
F &= -6\overline{K}\left(1 - \cos\left(\mathrm{qa}\right)\right)\omega_{n1}^4\omega_{n2}^2.
\end{aligned}
\tag{23}
$$

Similar to the explanations given for the one-degree-of-freedom model, Equation (22) shows the relationship between ω and qa. By plotting this equation, the dispersion curves are then available. By replacing $\mathrm{qa} = \pi$ in Equation (22), the expressions for the starting frequencies can be achieved as follows:

$$
\begin{aligned}
F_{s1} &= \sqrt{\frac{H}{3A} - \frac{1}{2}\left(\frac{C}{B} + B\right)},\\
F_{s2} &= \sqrt{\frac{H}{3A} + \left(\frac{C}{B} + B\right)}.
\end{aligned}
\tag{24}
$$

Now, by substituting $\mathrm{qa} = 0$ in Equation (22), the correlations between the system parameters and ending frequencies are given by

$$
\begin{aligned}
F_{e1} &= \frac{\sqrt{K - \sqrt{L}}}{2A},\\
F_{e2} &= \frac{\sqrt{K + \sqrt{L}}}{2A},
\end{aligned}
\tag{25}
$$

where

$$
\begin{aligned}
A &= 2\overline{m}_2^2\overline{I} + 2\overline{m}_2^2 + 2\overline{m}_2\overline{I},\\
B &= \left(E + \left(\left(E + D - F\right)^2 - C^3\right)^{1/2} + D - F\right)^{1/3},\\
C &= \frac{1}{3A}\left(\frac{H^2}{3A} + G\right),\\
D &= \frac{GH}{6A^2},\\
E &= \frac{H^3}{27A^3},\\
F &= \frac{6K\omega_{n1}^4\omega_{n2}^2}{A},\\
G &= 16K\omega_{n1}^4 + \left(3K + 3K\overline{m}_1 - 8\overline{m}_2\overline{I}\right)\omega_{n1}^2\omega_{n2}^2,\\
H &= \overline{m}_2\omega_{n2}^2\left(\overline{m}_2 + \overline{m}_1 + 2\overline{I} + 2\overline{m}_1\overline{I}\right) + \omega_{n1}^2\left(-4\overline{K} - 2\overline{K}\overline{m}_2 + 8\overline{m}_2\overline{I}\right),\\
I &= \overline{m}_1^2\overline{m}_2^2\left(2\overline{I} + 1\right)^2 + \left(2\overline{m}_1\overline{m}_2^3 + 4\overline{m}_1\overline{m}_2^2\overline{I}\right)\left(2\overline{I} + 1\right) + \left(2\overline{I}\overline{m}_2 + \overline{m}_2^2\right)^2,\\
J &= 4\overline{K}\overline{m}_1\overline{m}_2^2\left(4\overline{I} + 5\right) + 8\overline{K}\overline{m}_1\overline{m}_2\left(\overline{I} - 1\right) + 16\overline{K}\overline{m}_2^2\left(\overline{I} + 1\right) + 8\overline{K}\overline{m}_2\overline{I} - 4\overline{K}\overline{m}_2^3,\\
K &= H - 8\overline{m}_2\overline{I}\omega_{n1}^2,\\
L &= 16\overline{K}\left(\frac{\overline{m}_2^2}{4} + \overline{m}_2 + 1\right)\omega_{n1}^4 + I\omega_{n2}^4 + J\omega_{n1}^2\omega_{n2}^2.
\end{aligned}
\tag{26}
$$

3. The Integrity of One and Two DOF Models

To verify the results of this study extracted by mathematical modeling, both elastic metamaterials are modeled and simulated in MSC-ADAMS software under the assumption of rigid dynamics, as shown in Figures 6–9. Furthermore, the frequency response analysis (FRA) is performed for both models and frequency diagrams are then plotted. In the following section, the transient specifications of the system are expressed by parameter Π and the ratio of the fifth cell displacement to the displacement of the first cell and then compared with numerical solutions.

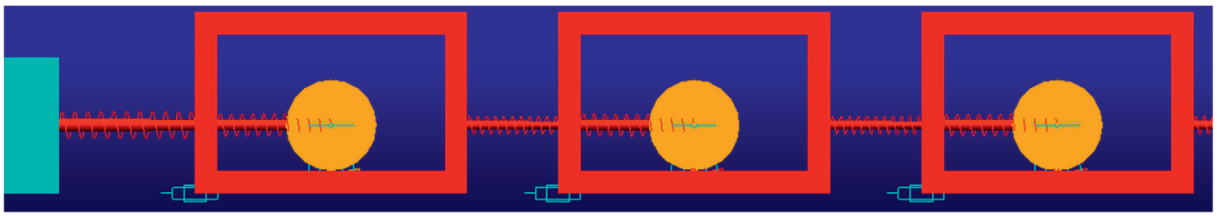

Figure 6: A schematic of the EMM arrangement of 1DOF model-MSC-ADAMS software.

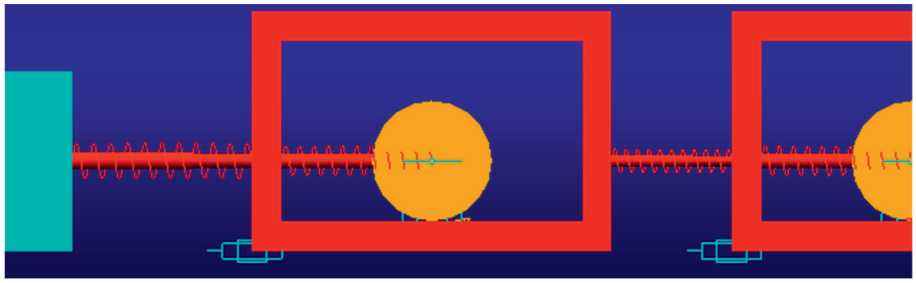

Figure 7: A schematic of a unite cell of 1DOF model-MSC-ADAMS software.

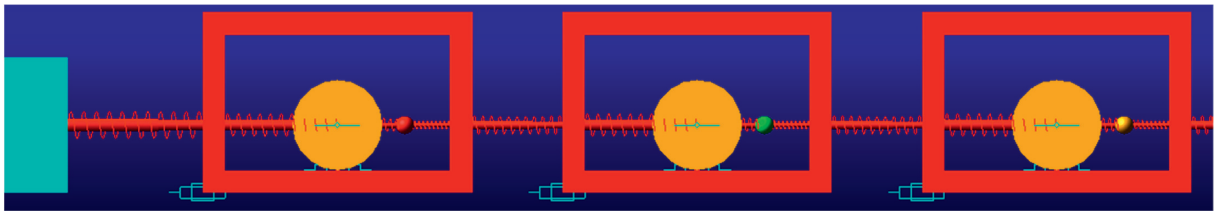

Figure 8: A schematic of the EMM arrangement of 2DOF model-MSC-ADAMS software.

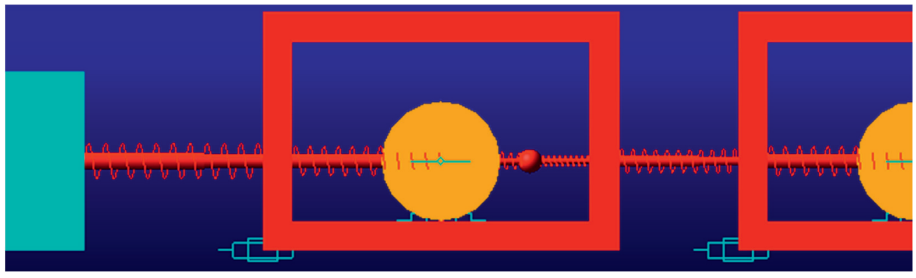

Figure 9: A schematic of a unite cell of 2DOF model-MSC-ADAMS software.

For numerical simulations, MATLAB/Simulink software is utilized, and the governing equations of proposed models are solved numerically. The block diagrams drawn by MATLAB/Simulink models are displayed in Figure 10. It is worth mentioning that each section in the diagram contains the equations governing the dynamics of a single cell.

For both models, the frequency response diagrams obtained from numerical solutions and simulations are plotted in Figures 11 and 12. As indicated, both analyses provide the same intervals for system bandgaps, demonstrating the satisfactory agreement between the results of both procedures which indicates the integrity of our mathematical modeling as well as numerical calculations.

4. Results and Discussion

After verifying the soundness of the numerical solutions, the dispersion characteristics and the effect of different system parameters on the bandgap intervals are comprehensively

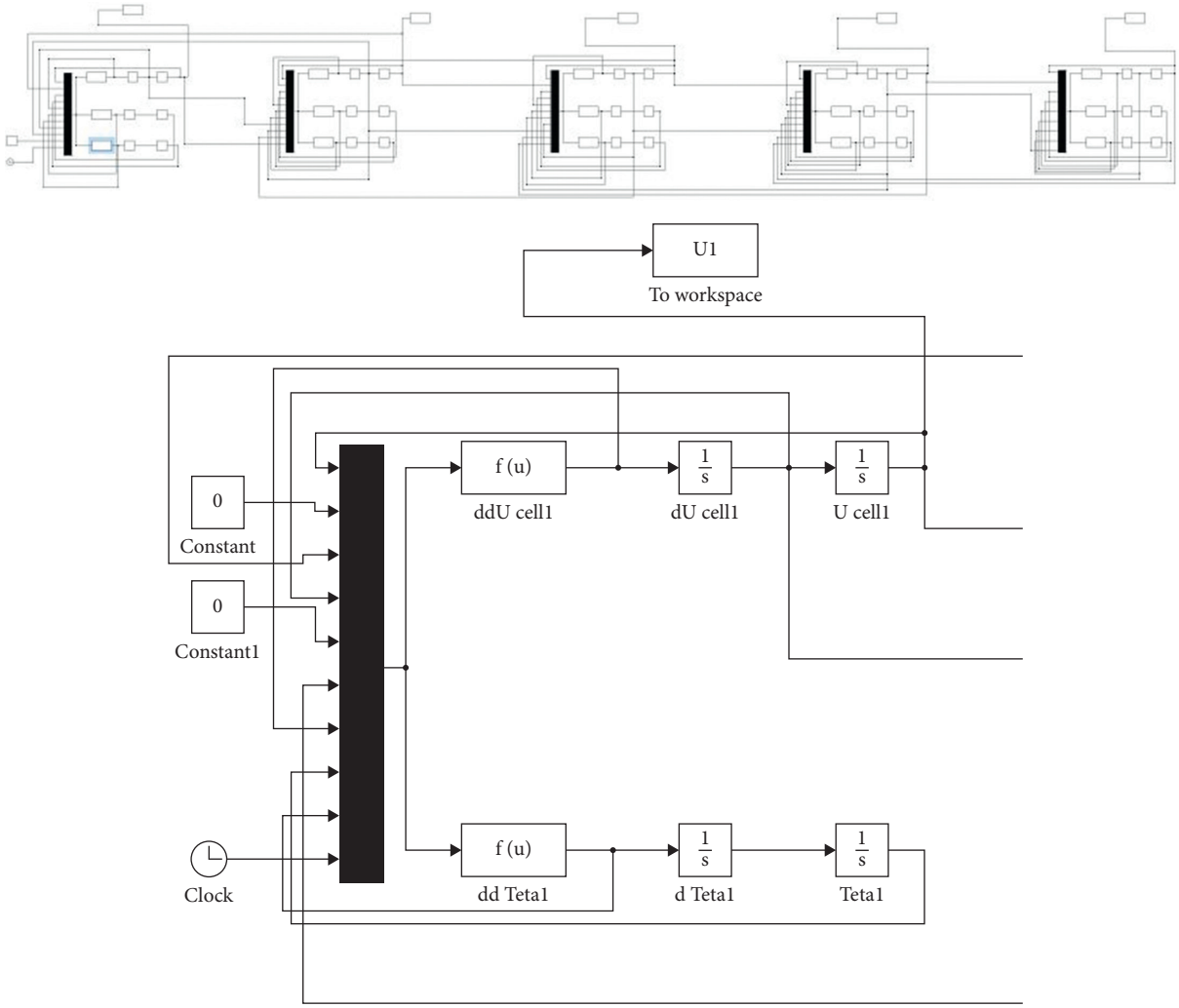

(a)

Figure 10: Continued.

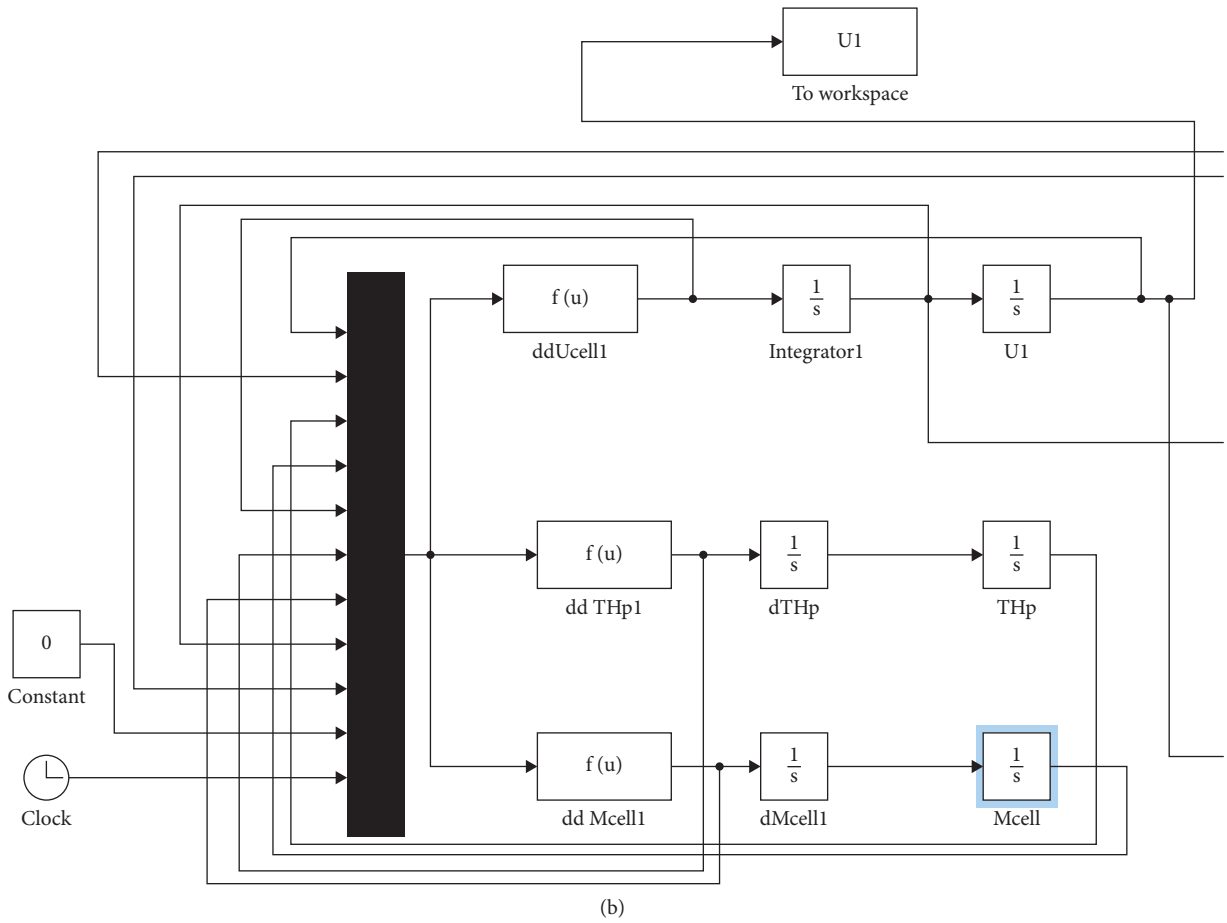

Figure 10: Block diagrams plotted in MATLAB/Simulink for the numerical solution of governing equations. (a) 1DOF model. (b) 2DOF model, array of cells (top) and a unit cell (bottom).

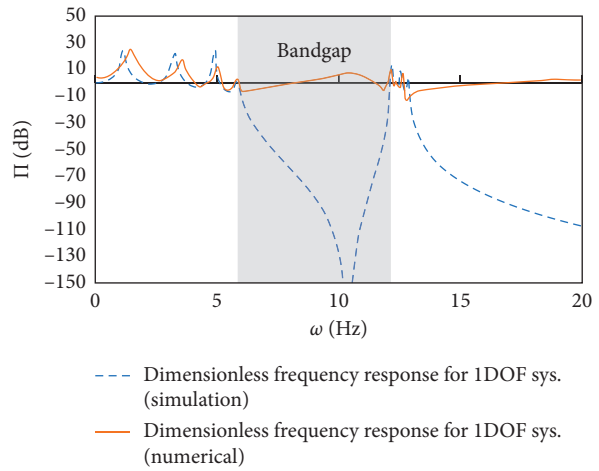

Figure 11: FRA for 1DOF model, comparison of numerical solution (MATLAB/Simulink) with simulation (MSC-ADAMS).

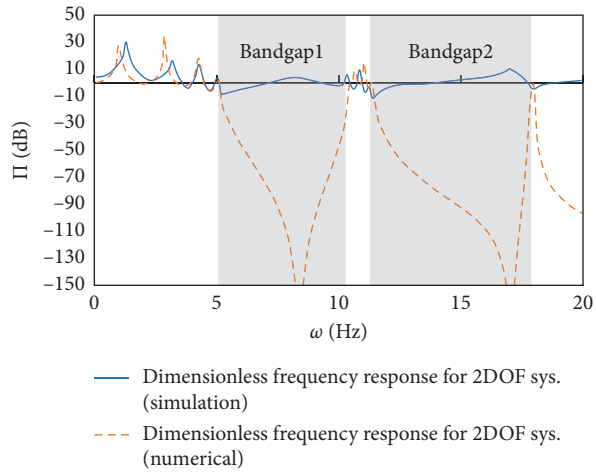

Figure 12: FRA for 2DOF model, comparison of numerical solution (MATLAB/Simulink) with simulation (MSC-ADAMS).

studied. In this section, it is aimed to examine the bandgaps of the introduced models and demonstrate in which conditions they can be extended or transmitted.

4.1. One DOF Model of EMM

4.1.1. Dispersion Curve for the 1DOF Model. Figure 2 shows the dispersion curves of the one-degree-of-freedom model, which shows the acoustic and optical wave modes as well as the bandgap interval. The values of the selected parameters are $M = 1.56, \widehat{I} = 1.5, \widehat{K} = 0.35$, and $\widehat{\omega}_n = 8.9$. Considering these parameters, the bandgap of the one-degree-of-freedom model is placed between the frequencies of 6.15 to 11.94 (Hz), which is the same as the frequency range obtained from Figure 11.

4.1.2. The Effect of System Parameters in the 1DOF Model. The surfaces drawn in Figure 13 exhibit the effect of different dimensionless parameters on the starting and ending frequencies of their corresponding bandgaps. The top and bottom surfaces indicate the starting and ending frequencies, respectively, and the distance between them indicates the bandgap interval of the 1DOF model. As can be seen in Figure 13, there is a direct relationship between the bandgap and the dimensionless stiffness, meaning that as the dimensionless stiffness increases, the bandgap is also enhanced. On the other hand, by increasing the dimensionless mass, the bandgap decreases. It is deduced that the stiffness parameter has a positive effect on the expansion of the bandgap and the effect of the mass parameter is to weaken the bandgap interval. Moreover, according to the illustrated results, in general, the dimensionless moment of inertia directly affects the bandgap range, which means that as the dimensionless moment of inertia increases, the bandgap of the model is also enlarged. Although the bandgap interval slightly decreases at the lower values, when the dimensionless moment of inertia takes the higher values, this interval is then enhanced satisfactorily.

4.2. 2DOF Model of EMM

4.2.1. Dispersion Curve for the 2DOF Model. In order to display the dispersion curves of the modified model with multiple resonators, one can solve Equation (22) for ω and extract the desired curves. The values of the selected parameters are $\overline{m}_1 = 1.04, \overline{m}_2 = 0.64, \overline{I} = 1.5$, and $\overline{K} = 2.86$, $\omega_{n1} = 4.2\,(\text{rad/s}), \omega_{n2} = 15.9\,(\text{rad/s})$. Considering the above parameters, the bandgap starting frequencies (F_{s1} and F_{s2}) are calculated by substituting qa = $\pm\,\pi$ in the acoustic and optical wave modes, respectively. The resulting plots are shown in Figure 14 by Ds(1) and Ds(2), respectively. In addition, the bandgap ending frequencies (F_{e1} and F_{e2}) are also extracted by replacing qa = 0 in two optical roots of Equation (22), respectively. The plotted results are illustrated in Figure 14 by Ds(2) and Ds(3), respectively. As indicated in Figure 14, the difference between the first starting frequency and the first ending frequency demonstrates the first bandgap, and the difference between the second starting frequency and the second ending frequency represents the second bandgap. According to the illustrated results in Figure 12, one can find that there is a small area between the first and second bandgaps. This consequence is also demonstrated in Figure 14 with a slight difference between the highest and lowest points of Ds(2). The slight difference leads to the flattening of the Ds(2) curve.

4.2.2. Comparison of Dispersion Curves for Two Models. As shown in Figure 15, by adding the concentrated mass and modifying the 1DOF model to a 2DOF model, two bandgaps are created in the dynamics of the new model, which allows us to reduce or suppress the vibrations of the modified system in more frequency ranges. From the comparison between the dispersion curves of both models, one can conclude that the first bandgap in the two-degree-of-freedom model starts and ends at lower frequencies than that of the one-degree-of-freedom model.

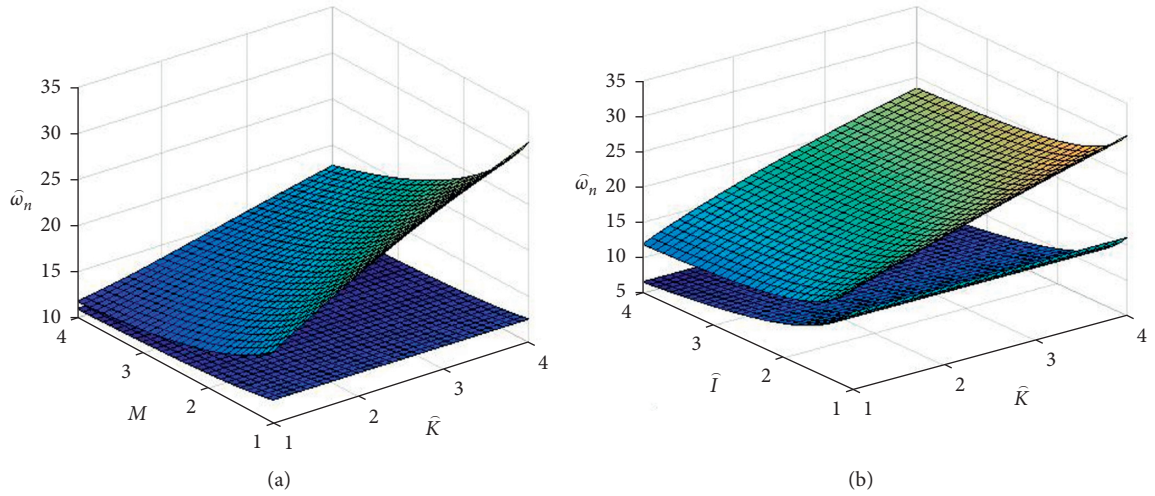

Figure 13: The effect of changing (a) $\widehat{K}$ and M and (b) $\widehat{K}$ and $\widehat{I}$ on the starting and ending frequencies of the bandgap for 1DOF model.

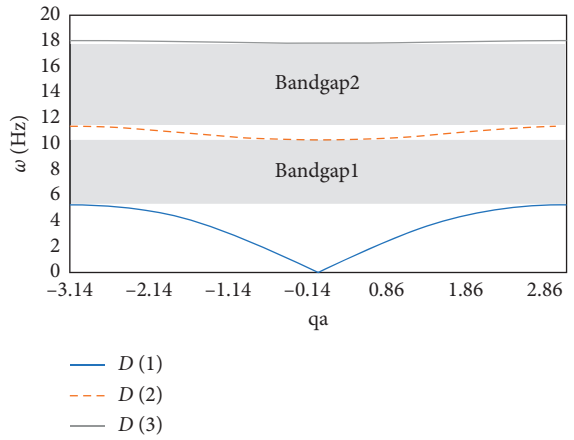

Figure 14: Dispersion curves for the 2DOF model.

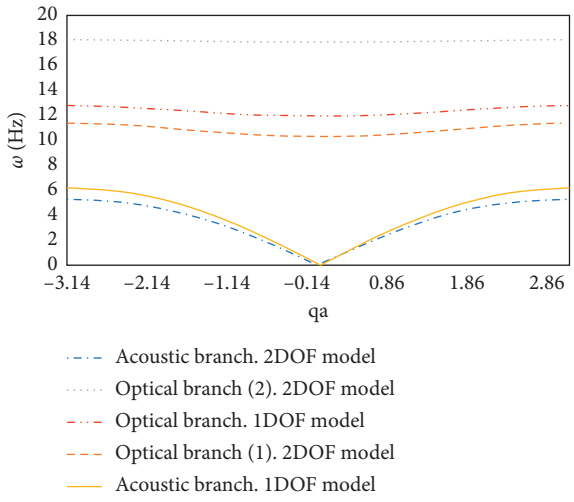

Figure 15: Comparison of dispersion curves in two models.

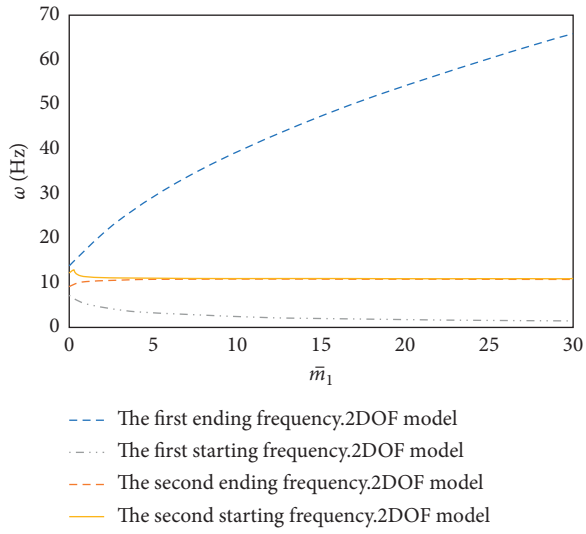

Figure 16: The effect of $\overline{m}_1$ parameter on bandgap for the 2DOF model.

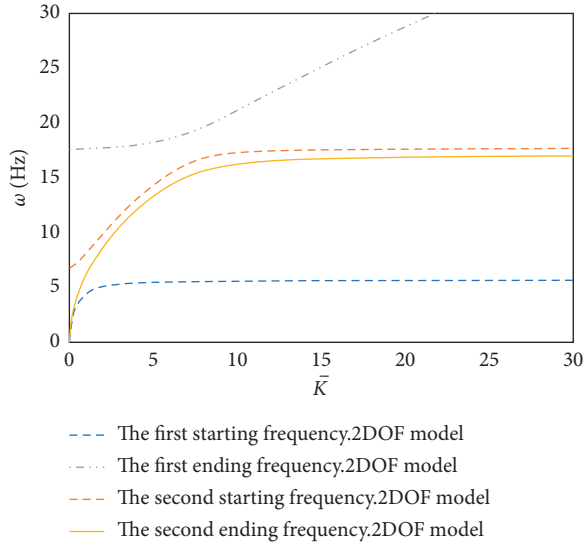

Figure 17: The effect of $\overline{K}$ parameter on bandgap for the 2DOF model.

4.2.3. The Effect of System Parameters in the 2DOF Model. Figure 16 displays well that when the parameter $\overline{m}_1$ shifts upward, the first starting frequency also increases and the first ending frequency reduces, which satisfactorily expands the first bandgap of the modified model. On the other hand, by increasing the first bandgap, the second one decreases and the starting and ending frequencies eventually reach a constant value.

With increasing the parameter $\overline{K}$, the first bandgap can be extended to cover a larger frequency range, as shown in Figure 17, although the first starting frequency will eventually approach a constant value. However, the change in the second bandgap of the model does not show the same trend, eventually converges to an almost constant value, and no longer changes significantly.

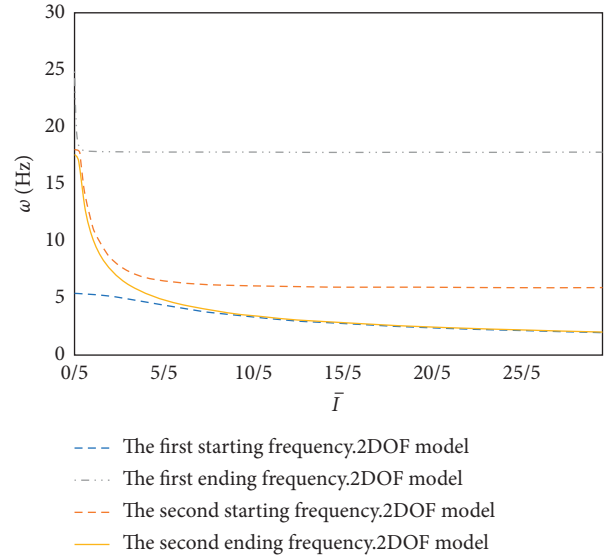

Figure 18: The effect of $\overline{I}$ parameter on bandgap for the 2DOF model.

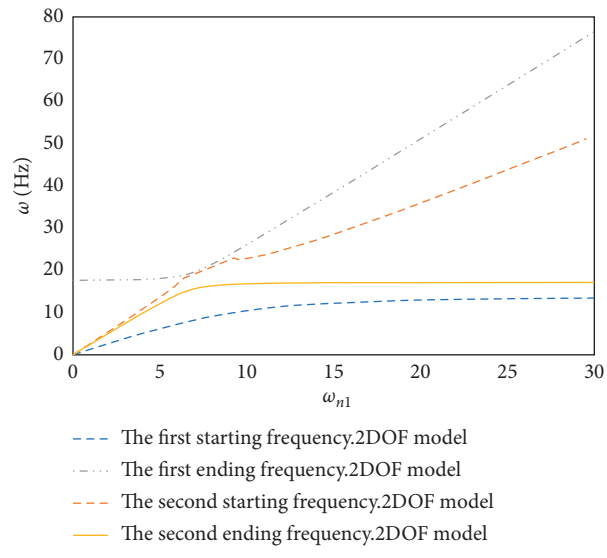

Figure 19: The effect of ω_{n1} parameter on bandgap for the 2DOF model.

For the sake of extending the first and second bandgaps of the modified model, the dimensionless moment of inertia $\overline{I}$ has to be increased. As indicated in Figure 18, by continuing the process of increasing the dimensionless moment of inertia, the first ending and the second starting frequencies will not change and take a constant value.

As the first and second local frequencies increase, the same behavior cannot be observed in the first bandgap of this model, although it decreases with small values and follows an increasing trend at higher values (see Figures 19 and 20). In general, it can be inferred that the first bandgap is expanded. Finally, it is found that with the increase of the first local frequency, the expansion of the second bandgap is not

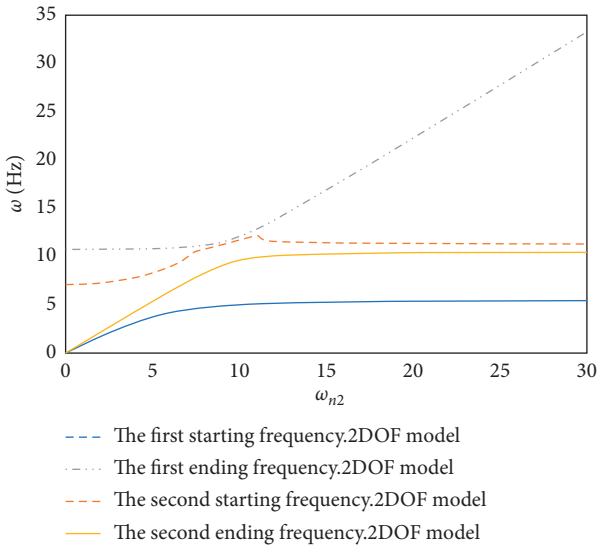

FIGURE 20: The effect of ω_{n2} parameter on bandgap for the 2DOF model.

uniform, although, in general, it becomes larger. Moreover, it should be pointed out that when the second local frequency increases, the second bandgap of the modified model is reduced.

5. Concluding Remarks

In this paper, at first, a new model of elastic metamaterials (1DOF model) involving a rack-and-pinion mechanism was presented. Then, by adding a concentrated mass, the model was modified by converting to a novel metastructure with multiple resonators in which more broadband bandgaps were produced. Different system parameters allow us to shift or expand the frequency ranges at which the system vibrations are reduced or eliminated by changing them. The influences of different system parameters on the bandgap intervals of the considered metamaterial are summarized as follows:

(i) By adding the concentrated mass and converting the model from 1DOF to 2DOF, two bandgaps are satisfactorily produced in the dynamics of the system

(ii) In the 1DOF model, in order to achieve the wider bandgap, in general, the dimensionless parameters $\widehat{I}$ and $\widehat{K}$should be increased or the dimensionless mass parameter M should be reduced

(iii) In the 2DOF model, the width of the first bandgap is enhanced by increasing the parameters $\overline{K}$, $\overline{I}$, $\overline{m}_1$, and ω_{n1} and decreasing ω_{n2}

(iv) In the 2DOF model, the width of the second bandgap is improved by increasing $\overline{I}$, ω_{n1}, and ω_{n2} or decreasing the parameter $\overline{m}_1$. No significant effect was demonstrated by varying the parameter $\overline{K}$

Data Availability

The data will be available upon request to the corresponding author.

Conflicts of Interest

The authors declare that they have no conflicts of interest.

Acknowledgments

H. M. Sedighi is grateful to the Research Council of Shahid Chamran University of Ahvaz for its financial support (Grant No. SCU.EM99.98).

References

[1] M. Gao, Z. Wu, and Z. Wen, "Effective negative mass nonlinear acoustic metamaterial with pure cubic oscillator," *Advances in Civil Engineering*, vol. 2018, Article ID 3081783, 15 pages, 2018.

[2] S. E. Mendhe and Y. P. Kosta, "Metamaterial properties and applications," *International Journal of Information Technology and Management*, vol. 4, no. 1, pp. 85–89, 2011.

[3] A. Valipour, M. H. Kargozarfard, M. Rakhshi, A. Yaghootian, and H. M. Sedighi, "Metamaterials and their applications: an overview," *Proceedings of the Institution of Mechanical Engineers, Part L: Journal of Materials: Design and Applications*, 2021.

[4] X. Zhou, J. Wang, R. Wang, and J. Lin, "Effects of relevant parameters on the bandgaps of acoustic metamaterials with multi-resonators multi-resonators," *Applied Physics A*, vol. 122, no. 4, pp. 1–8, 2016.

[5] H. Al Ba, D. DePauw, T. Singh, and M. Nouh, "Dispersion transitions and pole-zero characteristics of finite inertially amplified acoustic metamaterials," *Journal of Applied Physics*, vol. 123, pp. 1–12, 2018.

[6] S. Sang, "A new approach to generate local resonator for the application of acoustic metamaterials," *The Journal of the Acoustical Society of America*, vol. 142, 2017.

[7] H. H. Huang, C. T. Suna, and G. L. Huang, "On the negative effective mass density in acoustic metamaterials," *International Journal of Engineering Science*, vol. 47, no. 4, pp. 610–617, 2009.

[8] M. Nouh, O. Aldraihem, and A. Baz, "Metamaterial structures with periodic local resonances," *Health Monitoring of Structural and Biological Systems*, vol. 9064, pp. 1–11, 2014.

[9] A. H. Orta and C. Yilmaz, "Inertial amplification induced phononic band gaps generated by a compliant axial to rotary motion conversion mechanism," *Journal of Sound and Vibration*, vol. 439, pp. 329–343, 2019.

[10] B. S. Lazarov and J. S. Jensen, "Low-frequency band gaps in chains with attached non-linear oscillators," *International Journal of Non-Linear Mechanics*, vol. 42, no. 10, pp. 1186–1193, 2007.

[11] K. Wang, J. Zhou, D. Xu, and H. Ouyang, "Lower band gaps of longitudinal wave in a one-dimensional periodic rod by exploiting geometrical nonlinearity," *Mechanical Systems and Signal Processing*, vol. 124, pp. 664–678, 2019.

[12] J. S. Chen and I. Chien, "Dynamic behavior of a metamaterial beam with embedded membrane-mass structures," *Journal of Applied Mechanics*, vol. 84, no. 12, pp. 1–7, 2017.

[13] A. Casalotti, S. El-Borgi, and W. Lacarbonara, "Metamaterial beam with embedded nonlinear vibration absorbers," *International Journal of Non-Linear Mechanics*, vol. 98, pp. 32–42, 2018.

[14] X. Zhou, W. Jun, and R. Wang, "Band gaps in grid structure with periodic local resonator subsystems," *Modern Physics Letters B*, vol. 31, no. 25, 2017.

[15] G. L. Huang and C. T. Sun, "Band gaps in a multiresonator," *Journal of Vibration and Acoustics*, vol. 132, pp. 1–6, 2010.
[16] H. Sun, X. Du, and P. F. Pai, "Theory and experiment research of metamaterial beams for broadband vibration absorption," *Journal of Intelligent Material Systems and Structures*, vol. 21, no. 11, pp. 1085–1101, 2011.
[17] S. Xiao, T. Wang, T. Liu, C. Zhou, X. Jiang, and J. Zhang, "Active metamaterials and metadevices: a review," *Journal of Physics D: Applied Physics*, vol. 53, no. 50, Article ID 503002, 2020.
[18] Y. Y. Chen, M. V. Barnhart, J. K. Chen, G. K. Hu, C. T. Sun, and G. L. Huang, "Dissipative elastic metamaterials for broadband wave mitigation at subwavelength scale," *Composite Structures*, vol. 136, pp. 358–371, 2016.
[19] Z. Li, C. Wang, and X. Wang, "Modelling of elastic metamaterials with negative mass and modulus based on translational resonance," *International Journal of Solids and Structures*, vol. 162, pp. 271–284, 2019.
[20] A. H. Shirazi and H. M. Sedighi, "Physics of rack-and-pinion-inspired metamaterials with rotational resonators for broadband vibration suppression," *The European Physical Journal Plus*, vol. 135, no. 3, pp. 1–23, 2020.
[21] C. Comi and J.-J. Marigo, "Homogenization approach and bloch-floquet theory for band-gap prediction in 2D locally resonant metamaterials," *Journal of Elasticity*, vol. 139, no. 1, pp. 61–90, 2020.
[22] L. O'Faolain, "Photonic crystal cavities for optical interconnects," in *Optical Interconnects for Data Centers*, pp. 121–156, Woodhead Publishing, Cambridge, UK, 2016.